ACS Applied Materials & Interfaces

CuO functionalized silicon photoanodes for efficient photoelectrochemical water splitting devices

Yuanyuan Shi,[a,b] Carolina Gimbert-Suriñach,[b] Tingting Han,[a] Serena Berardi,[b] Mario Lanza,*[a] Antoni Llobet*[b,c]

One of the main difficulties for the technological development of photoelectrochemical (PEC) water splitting (WS) devices is the synthesis of active, stable and cost-effective photoelectrodes that ensure high performance. Here we report the development of a CuO-based photoanode, which shows an onset potential for the water oxidation of 0.53 V vs. SCE at pH 9, which implies an overpotential of only 75 mV, and high stability above 10 hours. The photoanodes have been fabricated by sputtering a thin film of Cu^0 on commercially available n-type Si wafers, followed by a photoelectrochemical treatment in basic pH conditions. The resulting CuO/Cu layer acts as: (i) protective layer to avoid the corrosion of nSi, (ii) p-type hole conducting layer for efficient charge separation and transportation, and (iii) electrocatalyst to reduce the overpotential of the water oxidation reaction. The low cost, low toxicity and good performance of CuO-based coatings can be an attractive solution to functionalize unstable materials for solar energy conversion

Broader Context

The exploitation of solar energy as a renewable energy source has become one of the most popular alternatives to the consumption of fossil fuels. Nevertheless, the intermittency and location-dependency of sunlight, as well as the low power conversion efficiency and the still high price of photovoltaic (PV) solar cells, are the main factors hindering the massive use of PV technology. Recently, the use of sunlight to split water to produce a clean fuel (*i.e.* hydrogen) has become very popular; in addtion this approach allows for the storage and transportation of energy potentially at a relatively low cost. This strategy can be achieved using photoelectrochemical devices enabling water splitting at the surface of semiconductor electrodes. However, in most semiconductors the water splitting chemical reaction is not fast enough, plus it decays quickly due to photocorrosion. Thus, the development of cheap passivating and catalytic coatings has become a major challenge. In this work, we present a solar water splitting device, which uses a n-type Si photoanode, protected with a CuO/Cu film. The photoanodes not only show excellent activity and stability, but also low toxicity and price, as they have been synthesized using an industry-compatible method. Our work opens the door to the use of CuO films for the development of water splitting devices.

Introduction

Photoelectrochemical (PEC) cells exploit the built-in potential generated at semiconductor-liquid junctions under illumination to drive uphill chemical reactions, such as the splitting of water (Eq. 1), which can be used to produce hydrogen fuel in a clean manner.[1] The transformation of sunlight into chemical energy via the formation of new chemical bonds is attractive because it allows solar energy to be stored and transported.[2] The overall electrochemical water splitting can be divided in two half reactions, the reduction and oxidation, also named hydrogen evolution reaction (HER, Eq.2) and oxygen evolution reaction (OER, Eq. 3), respectively:

Overall water splitting: $2H_2O \rightarrow O_2 + 2H_2$ ($\Delta E = 1.23$ V) (Eq. 1)
HER: $2H^+ + 2\ e^- \rightarrow H_2 \uparrow$ ($E^0_{red} = 0.00$ V vs. NHE) (Eq. 2)
OER: $2H_2O + 4h^+ \rightarrow O_2 \uparrow$ ($E^0_{ox} = 1.23$ V vs. NHE) (Eq. 3)

where the redox potential values are reported versus the normal hydrogen electrode, NHE. The OER is considered the bottleneck of the overall process, being thermodynamically and kinetically demanding. Thus, enormous research efforts have been invested on developing efficient photoanodes for the OER, to be coupled, in a possible water spitting PEC device, to a dark Pt cathode, performing the HER (Fig. 1). Several kinds of photoanodes have been used in this PEC set-up, including metal oxide semiconductors (Fe_2O_3, WO_3, $BiVO_4$, …), group III-V semiconductors (GaAs, GaP, InP, …) and amorphous silicon, all being excellent light absorbers and in most of the cases with good carrier mobility.[3-5] Among them, silicon is a particularly interesting candidate due to its low cost and good ability to absorb light. Unfortunately, silicon is only able to produce modest photocurrent densities of some $\mu A/cm^2$, which decay very fast (in the minutes time scale) due to premature corrosion.[6] The reason is that the thermodynamic oxidation potential of Si is less positive than that of water oxidation (1.23 V vs. NHE at pH 0), thus making it susceptible

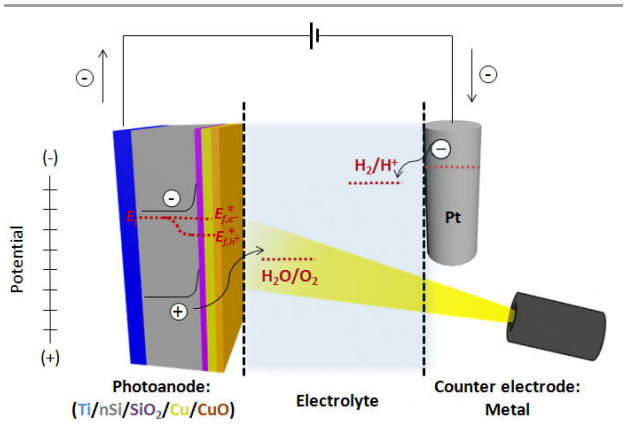

Fig. 1. Scheme of the PEC cell developed in this work. The cell consists on a Cu-protected nSi photoanode connected to a Pt counter electrode through a potentiostat. When the sunlight illuminates the surface of the photoanode, it induces charge separation. The photogenerated holes migrate to the surface and are used to produce O_2 from water. At the same time, the electrons promoted to the conduction band move to the counter electrode to reduce protons to hydrogen.

to self-oxidation when interfaced with aqueous electrolytes.[7] Therefore passivating the surface of silicon with a cheap coating that can serve as corrosion-resistant and water oxidation catalyst (WOC) has become one of the main challenges in this field.[8-16] Among all candidate materials, TiO_2 has shown outstanding performance in protecting Si and other III-V materials from oxidation,[4] but in those cases an additional WOC layer (film) is needed to boost the PEC reaction. Superstructures made of Ir/TiO_2[17] have shown water oxidation activity and stability in acid and basic conditions, while NiO_X/TiO_2[4] achieved even larger current densities, but only at pH 14. In fact, Ni-based coatings can be used as both anti-corrosion and WOC simultaneously. For example, Kenney et al.[18] evaporated a 2 nm Ni layer on a silicon wafer (with its native oxide), leading to inexpensive Ni/SiO_2/nSi photoanodes with extraordinary activity at pH 14 and enhanced stability at pH 9.5. Mei et al.[19] deposited Fe-modified NiOX films on np+-Si junctions (which notably enhance charge separation) and achieved continuous OER during 300 hours. Recently Lewis' group overcame that performance using 35-160 nm thick NiO_x coatings on np+-Si and achieved continuous OER during more than 50 days at pH 14.[20] Even though these devices show higher activity, the cost of these photoanodes is still high, as the fabrication of the np+ junction requires both implantation and thermal processes.

Due to its low cost and toxicity, copper is an attractive material from an industrial perspective, but its use in photoanodes for PEC WS-devices has never been reported. Recent advances showed that copper oxides,[21-25] as well as molecular copper complexes,[26-29] can be used to catalyse the electrocatalytic water oxidation reaction. Sun and coworkers[21] reported a continuous OER over 10 hours at pH 9 using a copper oxide catalyst electrodeposited on fluorine doped tin oxide (FTO), and a similar performance was achieved by Meyer and coworkers[22] by forming a CuO film on the surface of a Cu foil, but in both cases the water oxidation reaction was induced by applying a high external voltage. In this work, we report copper-based photoanodes for water oxidation that have been fabricated from Cu films sputtered on nSi photoanodes. The resulting devices work at very low overpotential (η = 75 mV) and stability (10 hours) at pH = 9.0. These findings point out the possibility of using copper-based composites as a promising photoanode for PEC-WS devices.

Experimental

Sample Preparation

All reagents were purchased from Aldrich unless otherwise stated. The fluorine doped tin oxide (FTO) coated glass was purchased from XopFisica (thickness, 2.3-3.0 mm; visible transmittance, 80-81.5%; resistance, 6-9 Ω/cm^2). Before the deposition and characterization tests, the FTO-coated glass was ultrasonically cleaned in water containing a cleaning detergent (Hellma), deionized water and ethanol, for 10 minutes each. Standard single side polished and phosphorous-doped [100] n-type silicon wafers (0.3-0.5 Ω•cm) were purchased from ProLog. Before all the deposition processes, the Si wafers were cleaned with acetone, ethanol and deionized water in an ultrasonic bath, for 10 minutes each. Cu^0 films with thicknesses of 5, 10, 15, 20 and 25 nm were deposited onto both FTO-coated glass and nSi photoanodes in the same vacuum chamber, by means of sputtering (ATC Orion 8-HV instrument, AJA International) at 100 W, with a deposition rate of 1.6 Å/s for 40, 80, 120, 160 and 200 s, respectively. An ohmic contact of 20 nm titanium was previously deposited onto the backside of the nSi wafers by e-beam evaporation (PVD75 Kurt J. Lesker). Copper tape was used to contact the working electrodes for electrochemical and PEC experiments.

Sample Characterization

All the samples were tested at room temperature in a standard three-electrode configuration with saturated calomel (SCE, saturated KCl) or Hg/Hg_2SO_4 (saturated K_2SO_4) reference electrodes and Pt wire as the counter electrode, using CHI 660D or CHI 660E potentiostats (CH Instruments, Inc.). The FTO samples were tested in a 20 mL one-compartment glass cell, and the nSi photoanodes in a 140 mL teflon cell, the areas exposed to OER were of ~1.0 and ~0.45 cm^2, respectively. In order to quantify the amount of O_2 produced, a two-compartment cell (in which anodic and cathodic sides are separated by a glass frit) was used. In this set-up, the Cu-coated nSi photoanodes were used as the working electrodes, Ag/AgCl (saturated KCl) as the reference and a Pt mesh as the counter electrode. All the cyclic voltammetry (CV) scans were collected with *i*R compensation at a scan rate of 100 mV/s, while the current density versus time traces were obtained without *i*R compensation. For comprehensive comparison, all redox potentials reported herein will be referenced versus SCE. An oxygen sensitive OXNP15121 Clark electrode (Unisense) was used to measure the photoproduced O_2 under air, and in turn to calculate the Faradaic efficiency. The electrolyte consisted of 0.2 M borate buffer solution (pH 9), obtained by mixing a 0.05 M $Na_2B_4O_7$ solution and a 0.2 M

H_3BO_3 solution in a ratio of 8:2 (v/v). All pH values were measured with a HI 4222 pH-meter (Hanna Instruments) using a calibrated Crison 5029 electrode (Crison Instruments). For the PEC characterization of the photoanodes, illumination was provided by 150 W Xe Arc Lamps (LS-150, ABET technology and 66906, Newport Corporation), equipped with a UV-light cut-off filter (λ < 400 nm) and calibrated to 1 sun (100 mW/cm^2) using a calibrated silicon photodiode at 25 °C.

UV-Vis characterizations were performed using a Cary 50 (Varian) spectrophotometer. The morphological characterization of the samples was performed by means of Transmission Electron Microscopy (TEM, JEOL, model 1011) and Scanning Electron Microscopy (SEM, FEI Quanta 200FEG). The chemical composition of the samples was analyzed by X-ray Photoelectron Spectroscopy (XPS), using a KRATOS Axis ultra-DLD spectrometer equipped with a monochromatic Mg Kα X-ray source (hν = 1283.3 eV).

Results and discussion

Copper films on FTO: electrocatalytic water oxidation

Metallic copper films of different thicknesses (5, 10, 15, 20 and 25 nm) were sputtered on FTO substrates. The resulting films are not homogenous as shown by the TEM images reported in Fig. S1, where it can be seen that the surface morphology depends on their thickness; the thinner Cu films appear to be rougher than the thicker ones. The electrocatalytic water oxidation ability of the sputtered copper electrodes was tested in 0.2 M borate buffer solution at pH 9. Unless otherwise stated, all the reported electrochemical measurements were performed in this electrolytic solution. As shown in Fig. 2a, regardless of their thickness, all the electrodes show similar onset potentials for the water oxidation reaction at 0.95 V vs. SCE (η = 495 mV), ~300 mV lower than that of the bare FTO. Current densities up to 7.5 mA/cm^2 were obtained at 1.1 V vs SCE. Similar results have been reported for other active CuO films, prepared using electrodeposition techniques,[21-22,24-25] suggesting that the copper oxide active species may have similar performances.

The stability of the generated CuO/Cu/FTO electrodes was assessed by means of successive CV scans, as well as by controlled potential electrolysis (CPE) at 1.1 V vs. SCE (Figs. 2b and S2a). In particular, Fig. 2b shows the remarkable stability of the current density trace of a 15 nm-thick CuO/Cu/FTO electrode. This sample maintains 80% of its activity after 12 hours of continuous OER. The small current decay observed is likely due to a loss of Cu^{2+} in solution, as evidenced by both electrochemical experiments on the electrolytic solution at the end of the CPE experiment (Fig. S3) and UV-Vis spectroscopy before and after 1 hour of CPE at 1.1 V vs. SCE (Fig. S2). The ability of the films to oxidize water, together with their good stability and transparency is a further evidence that the thin sputtered Cu layer can act as an anti-corrosion and WOC film.

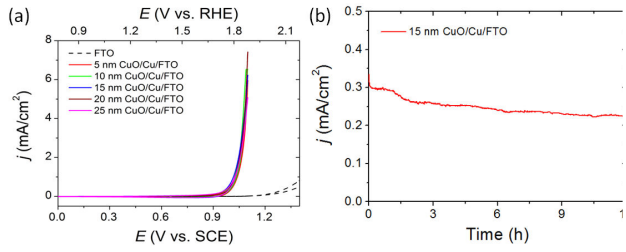

Fig. 2. Electrochemical water oxidation performances of CuO/Cu/FTO electrodes. (a) CVs of bare FTO (dashed black curve) and 5, 10, 15, 20 and 25 nm-thick Cu/FTO in 0.2 M borate buffer solution (pH 9). All the CV scans were obtained with iR compensation by using a SCE reference electrode and Pt counter electrode at a scan rate of 100 mV/s. (b) Current density traces obtained by controlled-potential electrolysis (CPE) at 1.1 V *vs*. SCE (without iR compensation) for a 15 nm CuO/Cu/FTO electrode in 0.2 M borate buffer solution (pH 9).

Copper films on nSi: photoelectrocatalytic water oxidation

Copper-coated nSi photoanodes were prepared by sputtering using the same methodology and parameters employed to prepare the Cu/FTO electrodes. The native SiO_2 on the nSi wafer was not etched, as it can serve as adhesive layer [18], and a layer of 20 nm Ti was evaporated on the back side of the nSi wafer, leading to Cu/SiO_2/nSi/Ti photoanodes. In total, nSi photoanodes with three different Cu0 thicknesses (5, 10 and 15 nm) were prepared, avoiding thicker films, which can hinder the photon absorption by silicon.

The current-density versus potential (*J-E*) plots in Fig. 3a obtained from CV scans for the as-grown 5 nm Cu/SiO_2/nSi/Ti photoelectrodes show very low activity and a large onset potential (~0.71 V vs. SCE). However, these Cu-coated nSi photoanodes can be activated by performing either (i) several

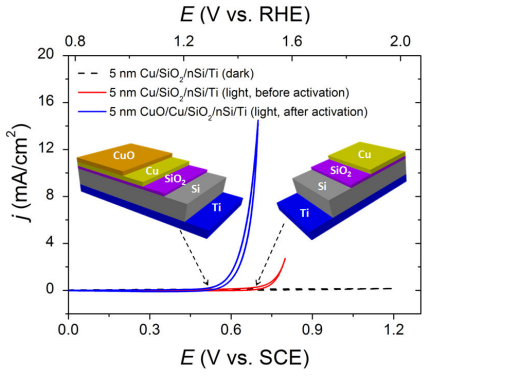

Fig. 3. Activation of the Cu/SiO_2/nSi/Ti photoanodes. (a) CV scans of 5 nm Cu/SiO_2/nSi/Ti before (red solid line) and after (blue solid line) activation under 1 sun illumination (see main text for activation details). The trace obtained in dark conditions is also reported (dashed black line). The CVs were obtained with iR compensation using a Pt counter electrode and Hg/Hg_2SO_4 reference electrode at a scan rate of 100 mV/s in 0.2 M borate buffer solution (pH 9). Insets: two 3D schematic representations, illustrating the activation process on the Cu/SiO_2/nSi/Ti photoanodes. The activation of the photoanode may be related to the formation of CuO on Cu layer.

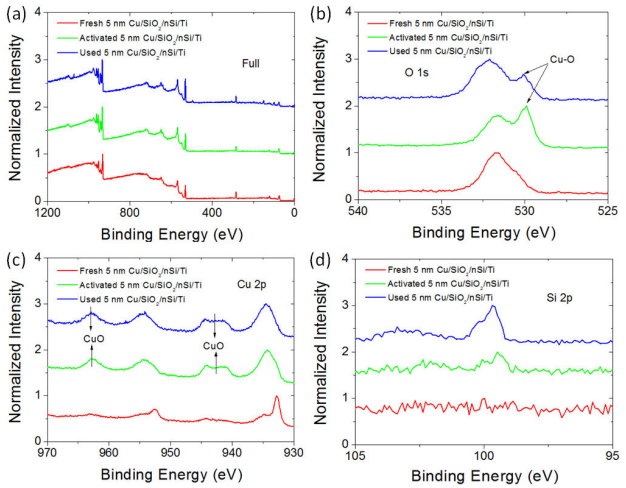

Fig. 4. (a) Overall XPS spectra of 5 nm Cu/nSi/SiO_2/Ti. Fresh sample (red), activated sample (green), degraded sample (blue). (b)-(d) XPS binding energy regions of O 1s, Cu 2p and Si 2p, respectively.

CV scans in a larger potential range (from -0.4 V to 0.8 V vs. SCE), (ii) chopped light linear sweep voltammetry (LSV) in the range from -0.4 to 0.9 V vs. SCE, or (iii) short time amperometric current vs. voltage (*I*-t) experiments (Fig. S4). After the activation process, a significant shift of the onset potential for OER (from ~0.71 V to ~0.53 V vs. SCE) and a remarkable increase of the current density (up to 14.5 mA/cm^2) can be obtained (compare red and blue lines in Fig. 3). The mechanism of the activation process for the Cu/SiO_2/nSi/Ti photoanodes is complex, possibly involving both soluble and insoluble products and multiple oxidation states (Cu^I, Cu^{II}, Cu^{III}, and/or Cu^{IV} species) depending on the applied potential.[22, 30,31] Two three-dimensional (3D) schematic representations of the electrode configuration are shown in the inset of Fig 3, indicating that the activation of the photoanodes may be related to the formation of CuO on the Cu layer.

In order to identify the changes induced during the activation process, the chemical composition of the 5 nm Cu/SiO_2/nSi/Ti photoanodes was analyzed by means of XPS. Fig. 4 shows the XPS peaks of O 1s, Cu 2p and Si 2p for the as-grown (red lines), activated (green lines) and used (blue lines) samples. The term "used" refers to a fresh 5 nm Cu/SiO_2/nSi/Ti photoanode that was exposed to 20 hours CPE at 0.8 V vs. SCE under 1 sun illumination (Fig. S7a). As reference, the wide binding energy regions of the samples are also exhibited in Fig. 4a. The O 1s binding energy region of fresh samples (red trace in Fig. 4b) shows just one component at 532 eV, corresponding to the oxygen on the surface.[32] This feature confirms the presence of a metallic copper component, since metallic Cu is reported to attract oxygen to the surface.[32] After the activation process (green trace in Fig. 4b), a new peak at 529 eV was observed, which can be attributed to Cu-O,[32] supporting the formation of a CuO film at the surface of the photoanodes. In the used sample (blue trace in Fig. 4b), the Cu-O peak at 529 eV is still present, but a decreasing in its intensity indicates a loss of the CuO, which may detach from the surface. On the other hand, in the Cu 2p binding energy region, the as-grown samples show two peaks at 932.7 eV and 952.6 eV (red trace in Fig. 4c), respectively assigned to 2p3/2 and 2p1/2 binding energies of Cu0 metal.[33] After the activation process, the 2p peaks shift to 934.4 eV and 954.2 eV (green trace in Fig. 4c), indicating the oxidation of copper to higher oxidation states, consistent with the formation of CuO, as already pointed out by the analysis of the O 1s region, and also reported for copper foils electrochemically exposed to high positive potentials, previously reported in the literature.[22] Finally, the clear appearance of the Si 2p peak in the spectrum of the used sample (blue trace in Fig. 4d) further supports that the decrease in activity observed in these photoanodes may be related to partial loss of the CuO film. The reported XPS analyses are fully reproducible, and similar results have been also obtained for the 10 and 15 nm thick counterparts (Figs. S5 and S6).

Fig. 5 reports the *J-E* plots measured for the CuO/Cu/SiO_2/nSi/Ti photoanodes (obtained from the activation of 10 nm Cu/SiO_2/nSi/Ti material) under dark and under 1 sun illumination (blue dashed and solid lines respectively) and the non-photoactive 10 nm thick CuO/Cu/FTO electrode (green solid line) at pH 9. As it can be observed, the effect of the CuO film on the FTO produces a remarkable decrease on the onset potential for OER (~300 mV, from 1.25 V to 0.95 V vs. SCE). When the CuO film is formed on the nSi/Ti substrate after the activation process, a remarkable further onset potential reduction of ~420 mV is achieved under illumination, leading to an absolute value of 0.53 V vs. SCE. This represents an impressive overpotential of 75 mV with

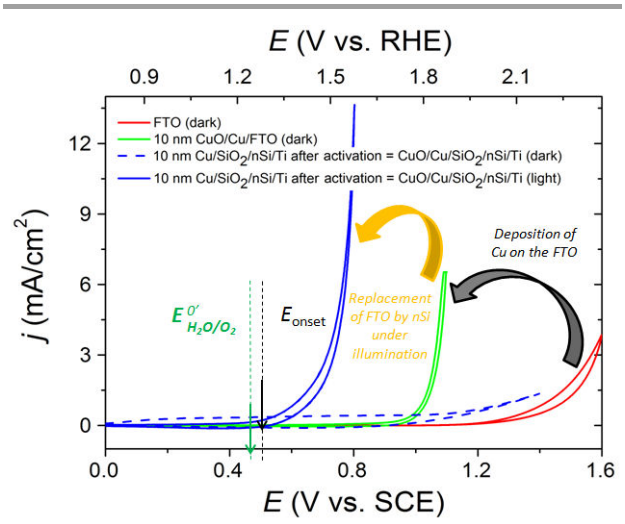

Fig. 5. Comparison of the onset potential for the water oxidation reaction by the different (photo) electrodes prepared in this work. Bare FTO (red line); 10 nm-thick CuO/Cu/FTO (green line); activated 10 nmCuO/Cu/SiO_2/nSi/Ti in the dark (dashed blue line) and under 1 sun illumination (solid blue line). All the CVs were recorded using a Pt mesh as the counter electrode and a SCE or Hg/Hg_2SO_4 as the reference electrode, with iR compensation at a scan rate of 100 mV/s in a 0.2 M borate buffer solution (pH 9).

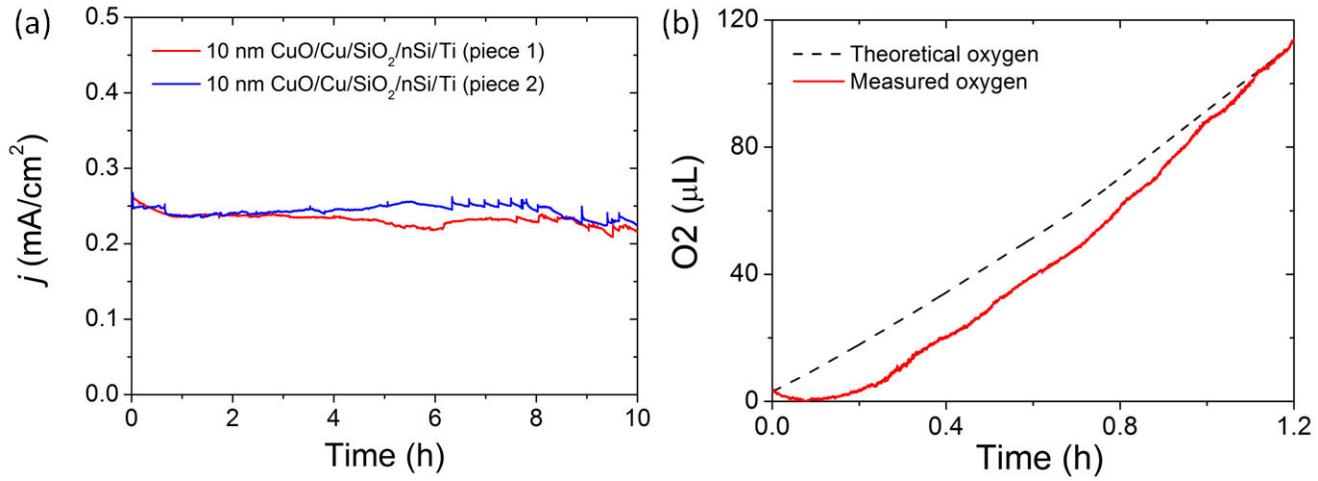

Fig. 6. Stability and faradaic efficiency of the activated 10 nm CuO/Cu/SiO_2/nSi/Ti photoanodes. (a) Current density versus time traces obtained by controlled potential electrolysis at 0.8 V vs. SCE on two different10 nm Cu/SiO_2/nSi/Ti photoanodes in 0.2 M borate buffer (pH 9) under 1 sun illumination, showing good reducibility. (b) Oxygen evolution trace (red solid line) measured with an activated 10 nm Cu/SiO_2/nSi/Tiin 0.2 M borate buffer (pH 9) at 0.85 V vs. SCE, under 1 sun illumination. From the measured and the theoretical (black dashed line) oxygen amounts, a ~100 % faradaic efficiency can be calculated. Both (a) and (b) were obtained without iR compensation, illuminated by a simulated 1 sun and using a Pt mesh as counter electrode. A one-compartment cell made of Teflon and a SCE reference electrode were used for tracing the current density (a) and a two-compartments glass cell and a Ag/AgCl reference electrode were used for the oxygen detection experiment (b).

regard to thermodynamic value.

The long-term stability of the produced photoanodes was tested by means of CPE experiments at 0.8 V vs. SCE. Fig. 6a shows the current density traces obtained for two activated 10 nm CuO/Cu/SiO_2/nSi/Ti photoanodes, showing excellent reproducibility and negligible variability. Once activated, both the photoanodes are stable for 10 hours at a constant current density of 0.24 mA/cm^2 under PEC conditions. The overall (≥ 20 hours) CPE plots for 5, 10 and 15 nm-thick Cu/SiO_2/nSi/Ti photoanodes indicate that the activation process (i.e. the formation of the CuO film) is needed for all Cu thicknesses, and that thicker films need a longer activation process (Fig. S7). The activation of the photoanodes takes place in a characteristic two-steps process: (i) a reduction of the initial current, probably related to a decreased conductivity associated to the transition from metallic Cu to CuO; and (ii) a current increase probably related to the formation of the CuO WOC film that boosts the OER and generates large current intensities. After that, the performance of the photoanodes becomes stable during long periods of time (up to 10 hours).

The surface of the samples has been further analysed by SEM (Fig. S8). While fresh 10 nm Cu/SiO_2/nSi/Ti photoanodes display very flat surfaces, the same samples after 37 hours CPE tests appear to be covered by nanoparticles. However, depending on the analysed region of the photoanode surface, a partial depletion of the number of CuO nanoparticles can be observed (e.g. in Fig. S8d), confirming that material loss is the major cause of current drop after long-term stability tests of this kind of photoanodes.

Finally, in order to prove that the photocurrent observed in the CPE experiments with the CuO/Cu/SiO_2/nSi/Ti photoanodes is actually due to the water oxidation reaction, a quantitative O_2 measurement was performed, using an oxygen gas sensor (Clark electrode). Fig. 6b shows the O_2 evolution profile obtained with an activated 10 nm CuO/Cu/SiO_2/nSi/Ti, held at a constant potential of 0.85 V vs. SCE, under simulated 1 sun illumination. A ~100% Faradaic efficiency can be calculated considering the theoretical and actual volume of O_2 produced (respectively, black dashed and red solid lines in Fig. 6b). The small delay in the experimental measurement of the evolved O_2 by the Clark electrode with regard to the measured current is due to the slow diffusion of oxygen into the membrane of the electrode sensor.

Conclusions

In conclusion, we have fabricated nSi photoanodes for PEC water splitting devices using for the first time CuO as water oxidation catalyst at the surface of a semiconductor. The devices show high activity at an impressively low overpotential of 75 mV. Furthermore they are stable for over 10 hours under 1 sun illumination in 0.2 M borate buffer at pH 9, with Faradic efficiencies close to 100%. Compared to the copper-based FTO electrode, the CuO-coated nSi photoanode shows an onset potential decrease for the OER of 420 mV under 1 sun illumination, which clearly highlights the advantages of this approach.

Finally it is important to stress here that the photoelectrodes described in the present work are made of Copper that is a cheap, earth-abundant and low toxicity metal. Furthermore all the operations carried out for the construction of the photonade are an industrially compatible and thus could be easily scale up for commercial applications. It thus offers a promising solution for the generation of clean and sustainable solar fuel. The conclusions section should come in this section at the end of the article, before the acknowledgements.

Acknowledgements

The start-up funding from Soochow University (China), MINECO (CTQ-2013-49075-R, SEV-2013-0319; CTQ-2014-52974-REDC), "La Caixa" foundation and AGAUR (2014-SGR-915) are acknowledged for financial support. C.G.S is grateful to AGAUR for a "Beatriu de Pinós" postdoctoral grant. S.B. is grateful to the ICIQ-IPMP Marie Curie COFUND Project (291787ICIQ-IPMP). European COST actions, CM1202 and CM1205 are also gratefully acknowledged.

References

1 N. S. Lewis and D. G. Nocera, *Proc. Natl. Acad. Sci. U.S.A.,* 2006, **103**, 15729-15735.
2 J. A. Turner, *Science,* 2013, **342**, 811- 812.
3 S. Hu, C. Xiang, S. Haussener, A. D. Berger and N. S. Lewis, *Energy Environ. Sci.,* 2013, **6**,2984-2993.
4 S. Hu, M. R. Shaner, J. A. Beardslee, M. Lichterman, B. S. Brunschwigand N. S. Lewis, *Science,* 2014, **344**, 1005-1009.
5 R. Liu, Z. Zheng, J. Spurgeon and Xiaogang Yang, *Energy Environ. Sci.,* 2014, **7**,2504.
6 A. Q. Contractor and J. O. M. Bockris, *Electrochim. Acta,* 1984, **29**, 1427-1434.
7 S. Chen, and L.-W. Wang, *Chem. Mater.,* 2012, **24**, 3659-3666.
8 M. G. Walter, E. L. Warren, J. R. McKone, S. W. Boettcher, Q. Mi, E. A. Santori and N. S. Lewis, *Chem. Rev.,* 2010, **110**, 6446-6473.
9 M. Pourbaix, Atlas of Electrochemical Equilibria in Aqueous Solutions (National Association of Corrosion Engineers, Houston, TX, ed. 2, **1974**).
10 H. Gerischer, *Faraday Discuss. Chem. Soc.,* 1980, **70**, 137-151.
11 K. Sivula, *J. Phys. Chem. Lett.,* 2013,**4**, 1624-1633.
12 B. Klahr, S. Gimenez, F. Fabregat-Santiago, J. Bisquert andT. W. Hamann, *J. Am. Chem. Soc.,* 2012, **134**, 16693-16700.
13 T. Hisatomi, F. Le Formal, M. Cornuz, J. Brillet,N. Tetreault, K. Sivula and M. Gratzel, *Energy Environ. Sci.,* 2011, **4**, 2512-2515.
14 M. Liu, C.-Y. Nam, C. T. Black, J. Kamcev and L. Zhang, *J.Phys. Chem. C.,* 2013, **117**, 13396-13402.
15 Z. Li, W. Luo, M. Zhang, J. Feng and Z. Zou, *Energy Environ. Sci.,* 2013, **6**, 347-370.
16 Z. Zhang, R. Dua, L. Zhang, H. Zhu, H. Zhang and P. Wang, *ACS Nano,* 2013, **7**, 1709-1717.
17 Y. W. Chen, J. D. Prange, S. Dühnen, Y. Park, M. Gunji, C. E. D. Chidsey& P. C. McIntyre, *Nat.Mater.,* **2011**, 10, 539-544.
18 M. J. Kenney, M. Gong, Y. Li, J. Z. Wu, J. Feng, M. Lanza & H. Dai, *Science,* 2013, **342**,836-840.
19 B. Mei, A. A. Permyakova, R. Frydendal, D. Bae, T. Pedersen,P. Malacrida, O. Hansen,I. E. L. Stephens, P. C. K. Vesborg, B. Segerand I. Chorkendorff,*J. Phys. Chem. Lett.,* 2014, **5**, 3456-3461.
20 K. Sun, M. T. McDowell, A. C. Nielander, S. Hu, M. R. Shaner,F. Yang, B. S.Brunschwig and N. S. Lewis, *J. Phys. Chem. Lett.,* 2015, **6**, 592-598.
21 F. Yu, F. Li, B. Zhang, H. Li and L. Sun, *ACS Catal.,* 2015, **5**, 627-630.
22 J. Du, Z. Chen, S.Ye, B. J. Wiley and T. J. Meyer, *Angew. Chem. Int. Ed.,* 2015, **54**, 2073-2078.
23 Z. Chen and T. J. Meyer, *Angew. Chem. Int. Ed.,* 2013, **52**, 700-703; *Angew. Chem.,* 2013, **125**, 728-731.
24 X. Liu, H. Jia, Z. Sun, H. Chen, P. Xu and P. Du, *Electrochem. Commun.,* 2014, **46**, 1-4.
25 X. Liu, S. Cui, Z. Sun and P. Du, *Electrochim. Acta*, 2015, **160**, 202-208.
26 M.-T. Zhang, Z. Chen, P. Kang and T. J. Meyer, *J. Am. Chem. Soc.,* 2013, **135**, 2048-2051.
27 S. M. Barnett, K. I. Goldberg and J. M. Mayer, *Nat. Chem.,* 2012, **4**, 498-502.
28 T. Zhang, C. Wang, S. Liu, J.-L. Wang and W. Lin, *J. Am. Chem. Soc.,* 2014, **136**, 273-281.
29 P. Garrido-Barros, I. Funes-Ardoiz, S. Drouet, J. B. Buchholz, F. Maseras and A. Llobet, *J. Am. Chem. Soc.*, 2015, **137**, 6758-6761.
30 G. Kear, B. D. Barkerand F. C. Walsh, *Corros. Sci.,* 2004, **46**, 109-135.
31 L. D. Burke, M. J. G. Ahern and T. G. Ryan, *J. Electrochem. Soc.,* 1990, **137**, 553-56.
32 Y.-K. Hsu, C.-H.Yu, Y.-C.Chen and Y.-G. Lin, *Electrochimica Acta,* 2013, **105**, 62-68.
33 C. D. Wanger, W. M. Riggs, L. E. Davis, J. F. Moulder and G. E. Muilenberg in Handbook of x-ray photoelectron spectroscopy: a reference book of standard data for use in x-ray photoelectron spectroscopy, PerkinElmer Corp., Physical Electronics Division, Eden Prairie, Minnesota, USA, 1979, p. 82.